Supporting Information

Characterization of Flame Synthesized Pd-TiO_2 Nanocomposite Catalysts for Oxygen Removal from CO_2-rich Streams in Oxy Combustion Exhausts

Sungyoon Jung, Nathan Reed, Gregory Yablonsky, and Pratim Biswas*

Aerosol and Air Quality Research Laboratory
Center for Aerosol Science and Engineering
Department of Energy, Environmental and Chemical Engineering
Washington University in St. Louis,
St. Louis, MO, 63130, USA

Submitted to Catalysis Science & Technology

May, 2021

*To whom correspondence should be addressed:

Tel: +1-314-935-5548; Fax: +1-314-935-5464

E-mail: *pbiswas@wustl.edu*

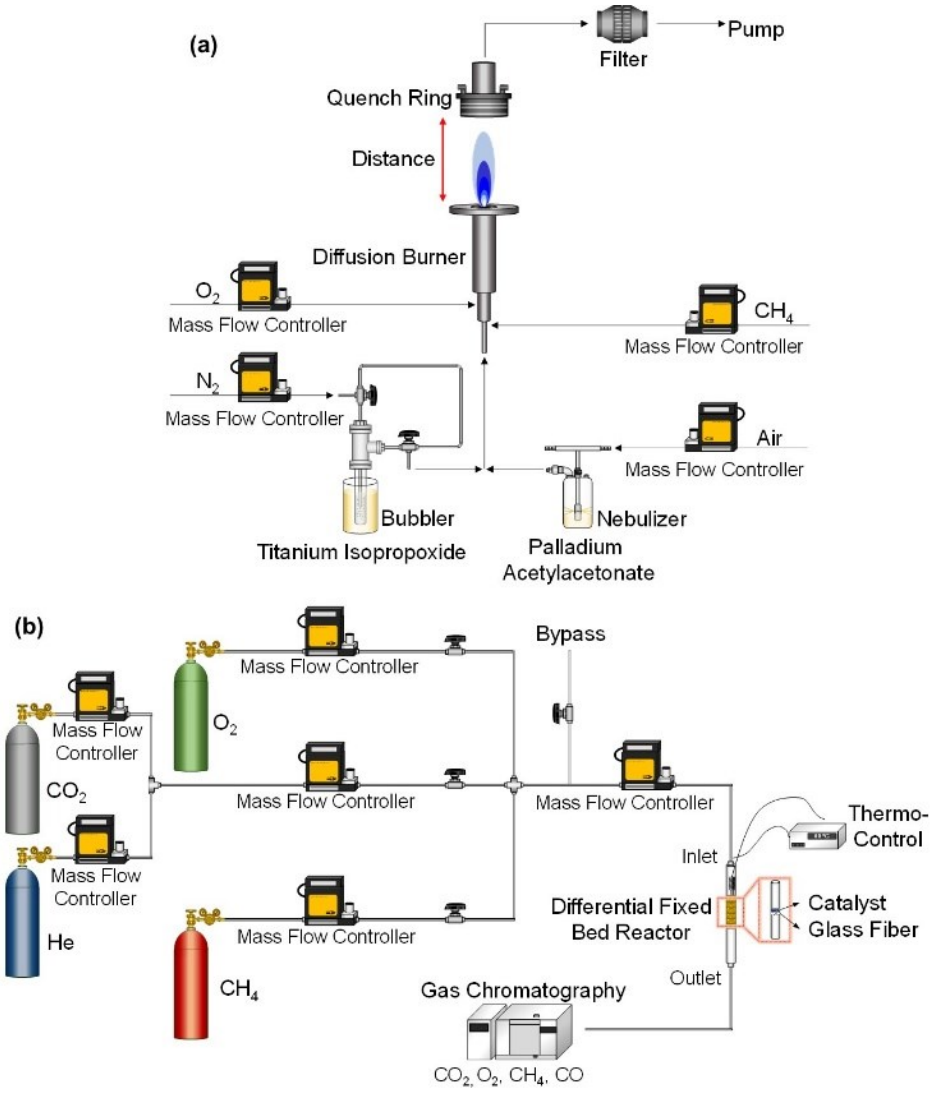

Fig. S1. Schematic diagram of (a) a system for Pd-TiO_2 catalyst synthesis and (b) a differential fixed-bed reactor system for O_2 removal test.

Synthesis of Pd-TiO_2 catalysts using a flame aerosol reactor (FLAR)

The experimental setup for synthesizing Pd-TiO_2 catalysts is shown in Fig. 1a. The flame aerosol reactor (FLAR) system includes a precursor feeding system (bubbler and nebulizer), a diffusion burner, and a quenching and collection system. The bubbler was used for feeding titanium tetra-isopropoxide (TTIP, 99.7%, Sigma-Aldrich) with an N_2 carrier gas (1 L min-1). The temperature of the oil bath in which the bubbler was placed was maintained at 323 K. The precursor delivery tubes were maintained at around 373 K. The saturated TTIP precursor vapor was introduced into the central port of the burner. Palladium acetylacetonate ($Pd(acac)_2$, 97%, Sigma-Aldrich) was used as a dopant precursor, and it was dissolved in xylene (reagent grade, Sigma-Aldrich) and acetonitrile (99.8%, Sigma-Aldrich) mixture (2:1, v/v). In this study, five different Pd-TiO_2 catalysts were synthesized by controlling the concentration of the Pd precursor solutions (0.5 mM ~3.0 mM). A three-jet Collison nebulizer was used to generate spray droplets, which were introduced to the central port of the burner. CH_4 and O_2 were introduced through the second and the outer port of the burner, respectively, with flow rates of 0.35 L min-1 and 2.5 L min-1. The distance between the quench ring and the top of the burner was fixed at 3.8 cm. The synthesized catalysts were collected using an isopore membrane filter.

Table S1 Total Pd loadings of fresh and spent catalysts as determined from FESEM-EDS analyses.

	Total Pd loading of fresh catalysts (wt%)	Total Pd loading of spent catalysts (wt%)
catalyst 1	0.21 ± 0.027	0.22 ± 0.038
catalyst 2	0.44 ± 0.041	0.42 ± 0.050
catalyst 3	0.75 ± 0.086	0.69 ± 0.098
catalyst 4	1.00 ± 0.072	0.99 ± 0.084
catalyst 5	1.25 ± 0.058	1.14 ± 0.153

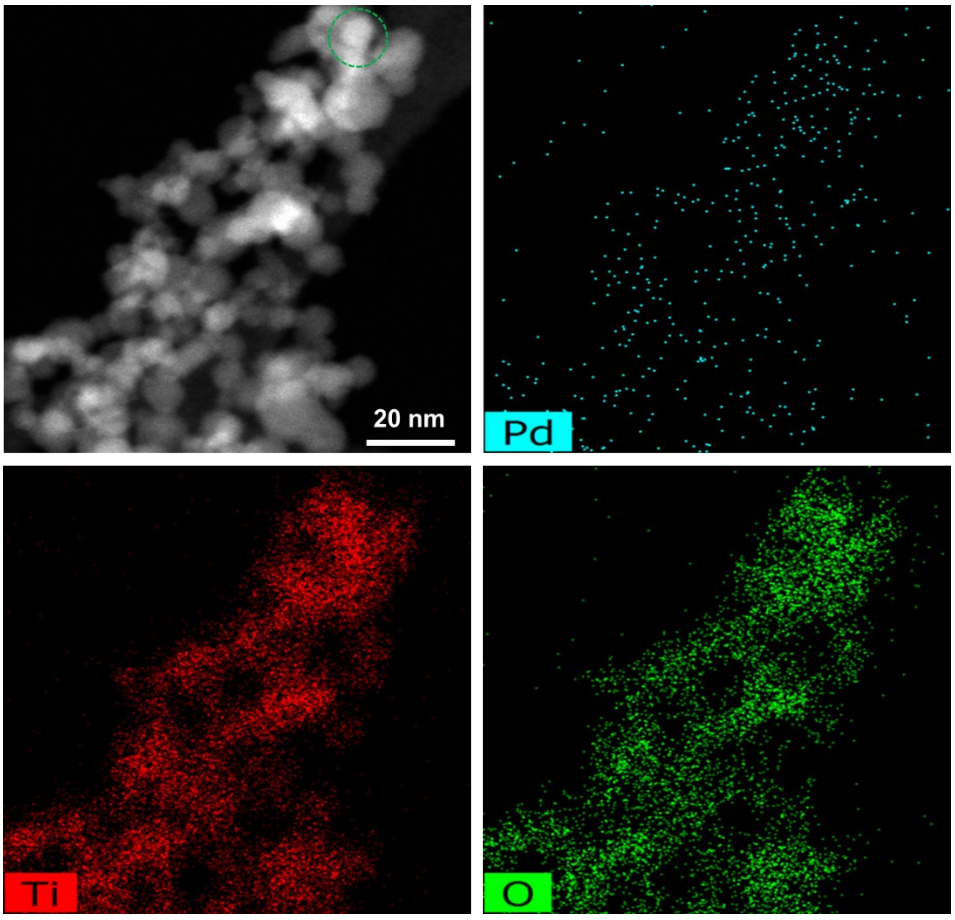

Fig. S2 EDS mapping of the fresh catalyst 4.

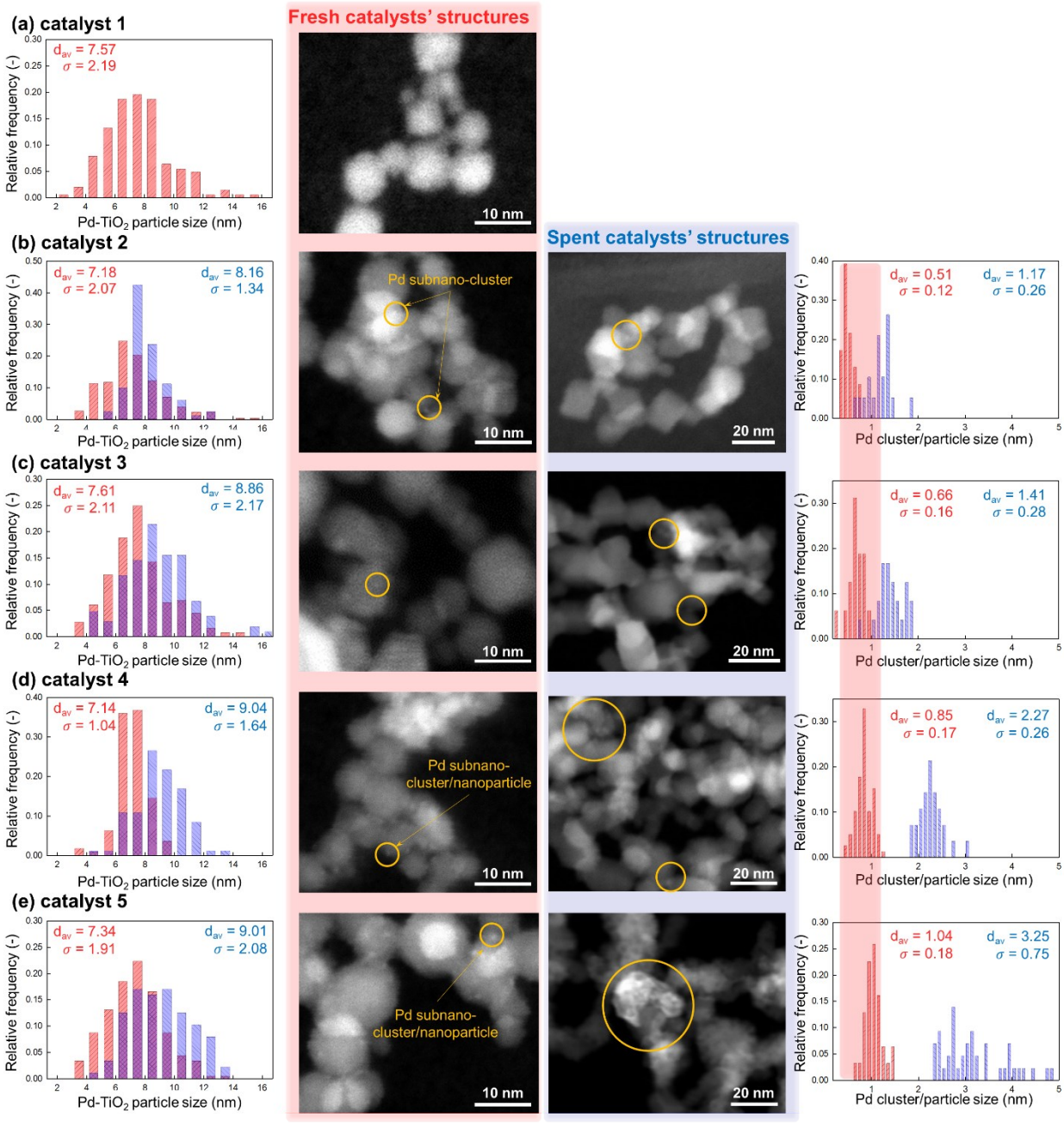

Fig. S3 Bulk Pd-TiO_2 nano particle and Pd subnano cluster/nano particle size distributions, and STEM images of a) catalyst 1, b) catalyst 2, c) catalyst 3, d) catalyst 4, and e) catalyst 5. Results related to the fresh catalysts are denoted with red-color and results related to the treated catalysts are shown with blue-color

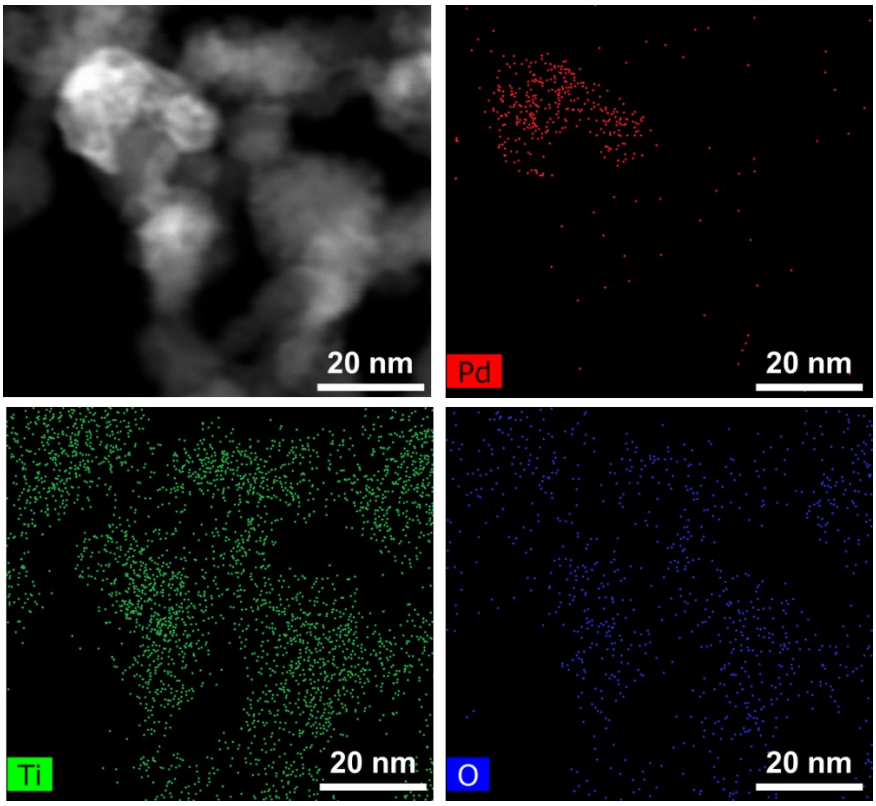

Fig. S4 EDS mapping of the spent catalyst 5.

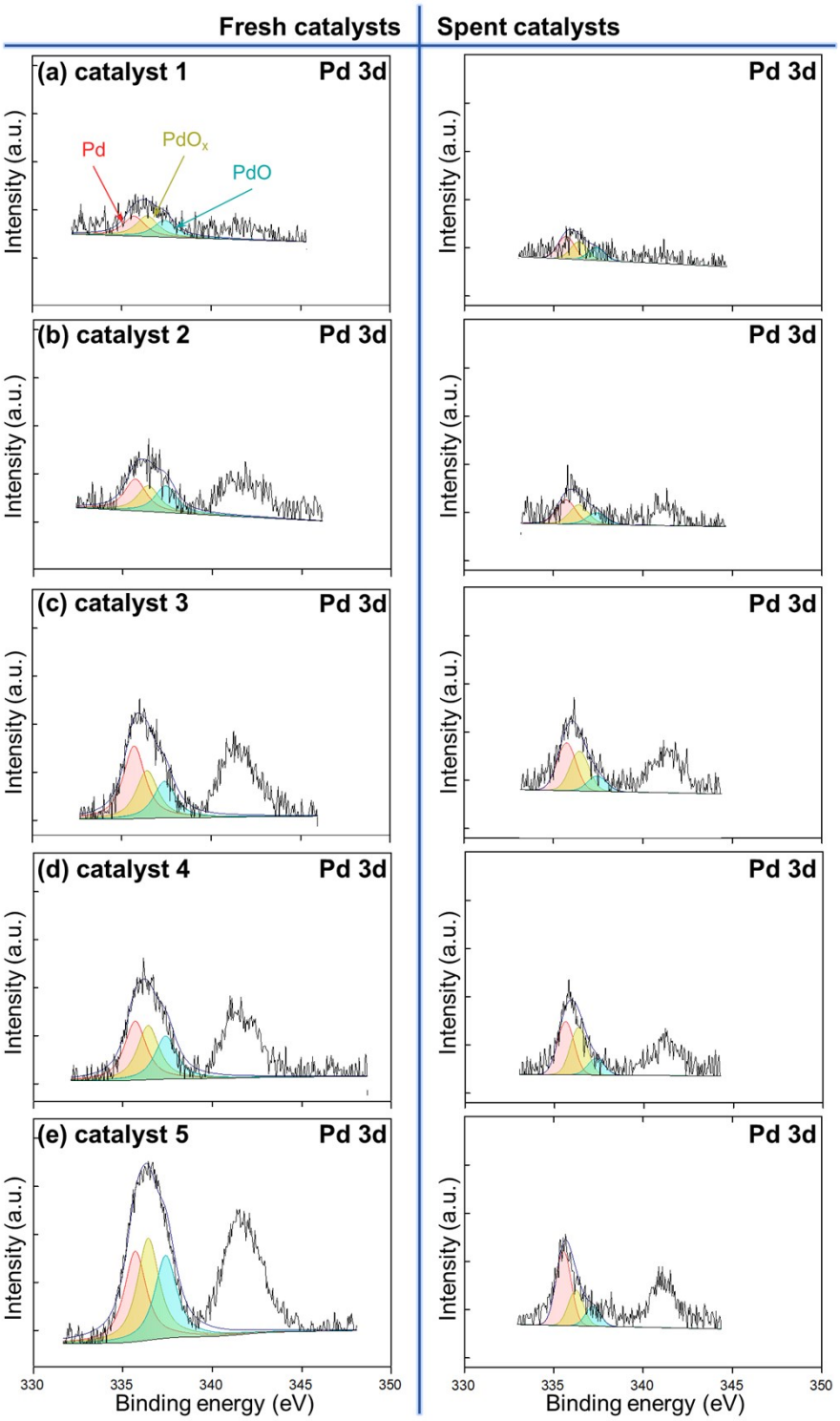

Fig. S5 XPS spectra of fresh and treated Pd-TiO_2 catalysts: Pd metal (red, 335.7 eV), PdO_x (gold, 336.42 eV), PdO (green, 337.4 eV).

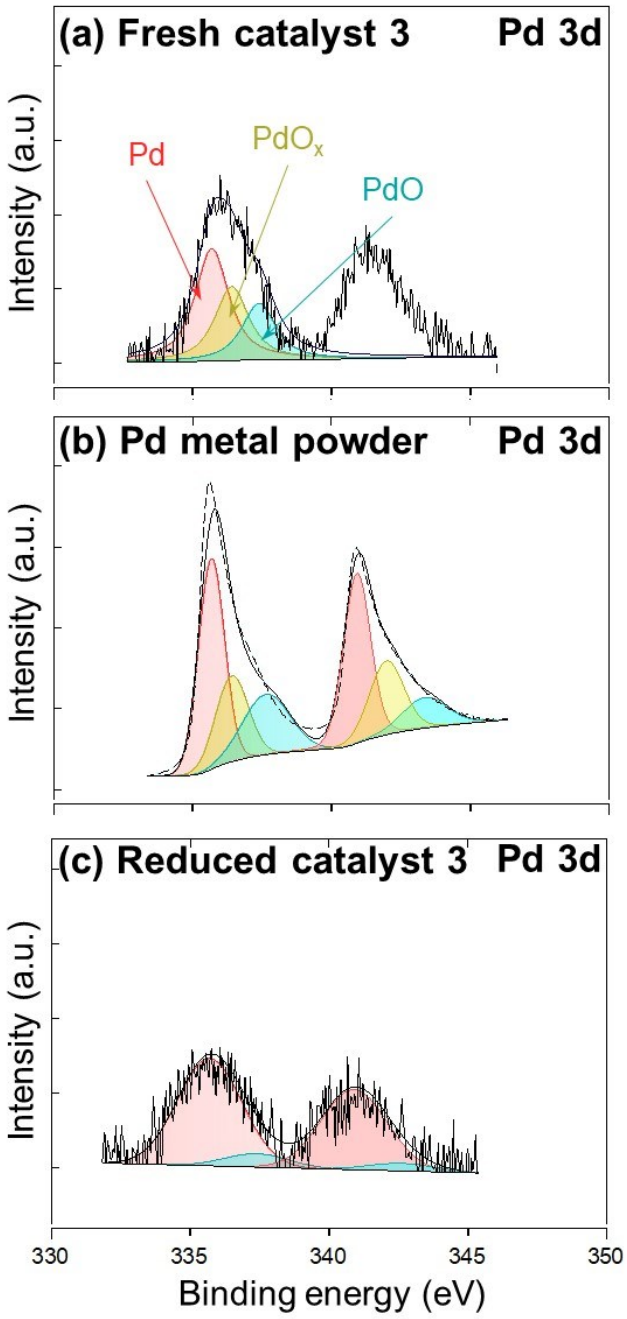

Fig. S6 XPS spectra of (a) fresh catalyst 3, (b) Pd metal powder, and (c) reduced catalyst 3: Pd metal (red, 335.7 eV), PdO_x (gold, 336.42 eV), PdO (green, 337.4 eV).

To validate the Pd species in the XPS data, the Pd species in Pd metal powder and the reduced catalyst 3 were additionally characterized. Pd metal powder was purchased from Sigma Aldrich

(Palladium, 326666). The reduced catalyst 3 was prepared by reducing the fresh catalyst 3 with hydrogen gas at 500 °C for 2 hrs. For a better comparison, original XPS data of fresh catalyst 3 is shown together with the obtained results (Figure S3a). As can be seen in Figure S3b, the purchased Pd metal powder contained three Pd species which are metallic Pd ($3d_{5/2}$=335.7 eV and $3d_{3/2}$=340.9 eV), intermediate Pd ($3d_{5/2}$=336.42 eV and $3d_{3/2}$=341.6 eV), and PdO ($3d_{5/2}$=337.4 eV and $3d_{3/2}$=342.6 eV). These deconvoluted Pd species in the Pd metal powder are consistent with those in the fresh catalyst 3 (Figure S3a). The existence of the oxidized Pd species (intermediate Pd and PdO) could be created during the sample preparation for the XPS analysis. The reduced catalyst 3 (Figure S3c) contained mostly metallic Pd and a small amount of PdO with binding energies at $3d_{5/2}$=335.7 eV and 337.4 eV and $3d_{3/2}$=340.9 eV and 342.6 eV, respectively. This result could indicate that the deconvoluted Pd species in the reduced catalyst 3 were consistent with those in the fresh catalyst 3 (Figure S3a) and catalyst 3 was successfully reduced. Therefore, these obtained XPS data could validate the Pd species in the prepared samples in the main paper.

Table S2 Fractions of metallic Pd, intermediate PdO_x, and PdO in the spent catalysts as determined from XPS analysis, and total surface area of metallic Pd ($TSA_{metallic\ Pd}$), intermediate PdO_x (TSA_{PdO_x}), and PdO (TSA_{PdO}).

	Metallic Pd (%)	PdO (%)	PdO_x (%)	$TSA_{metallic\ Pd}$ (cm^2)	TSA_{PdO} (cm^2)	TSA_{PdO_x} (cm^2)	$\frac{Tspent\ (\frac{I(Pd)}{I(Ti)})}{Fresh\ (\frac{I(Pd)}{I(Ti)})}$
catalyst 1	42.60 ± 1.12	24.07 ± 0.55	33.33 ± 0.65	-	-	-	0.920
catalyst 2	43.89 ± 0.16	21.27 ± 0.63	34.84 ± 0.47	85.68	68.49	86.16	0.422
catalyst 3	45.91 ± 0.75	15.80 ± 0.55	38.29 ± 0.86	124.70	70.78	131.74	0.417
catalyst 4	44.06 ± 0.65	16.38 ± 1.08	39.56 ± 0.95	105.61	64.75	120.12	0.352
catalyst 5	55.61 ± 1.44	14.77 ± 0.65	29.62 ± 1.37	-	-	-	0.206

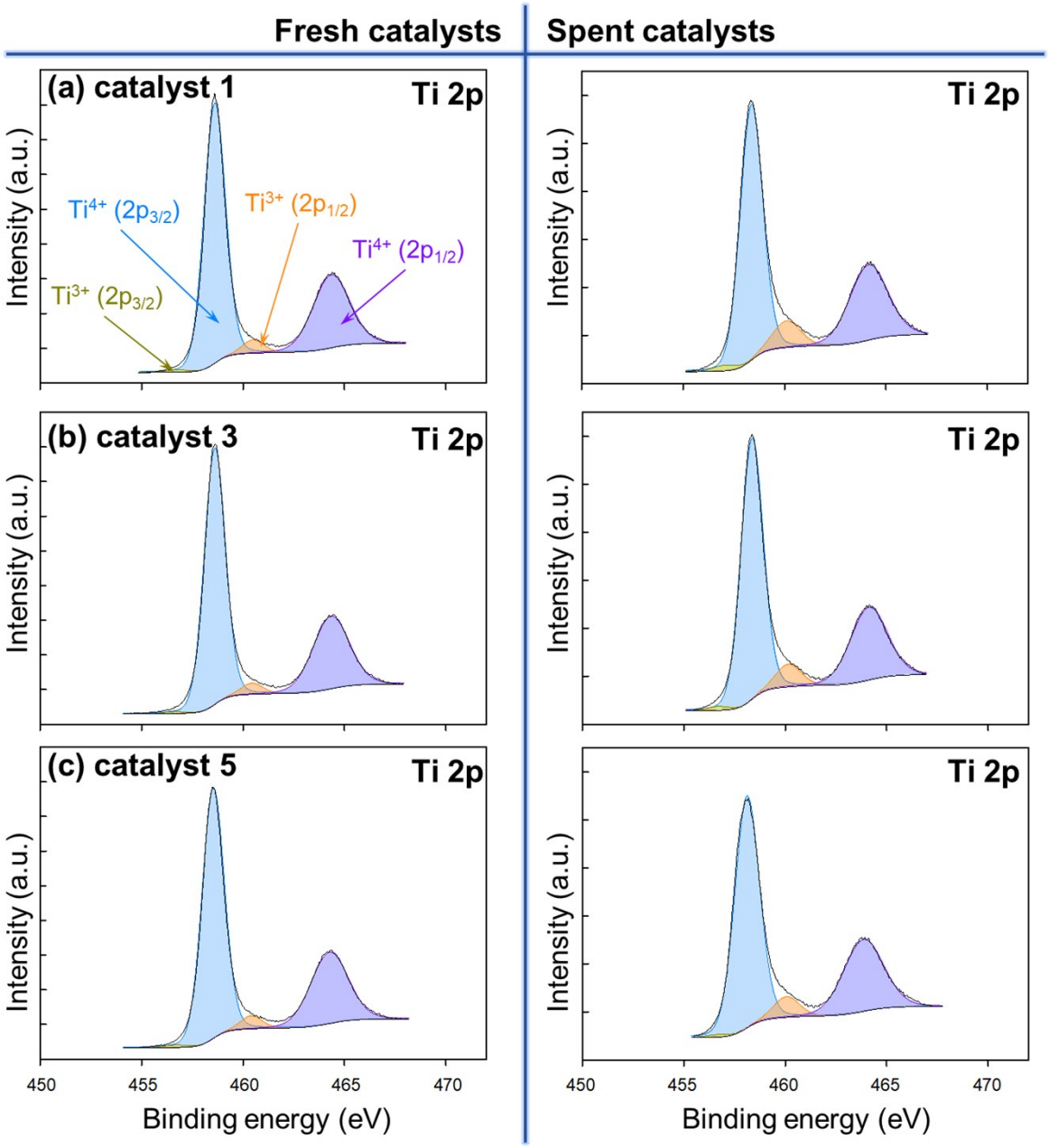

Fig. S7 XPS spectra of fresh and spent Pd-TiO_2 catalysts: Ti^{3+} ($2p_{3/2}$) (dark green, 456.7 eV), Ti^{4+} ($2p_{3/2}$) (blue, 458.5 eV), Ti^{3+} ($2p_{1/2}$) (orange, 460.3 eV), Ti^{4+} ($2p_{1/2}$) (purple, 464.2 eV).

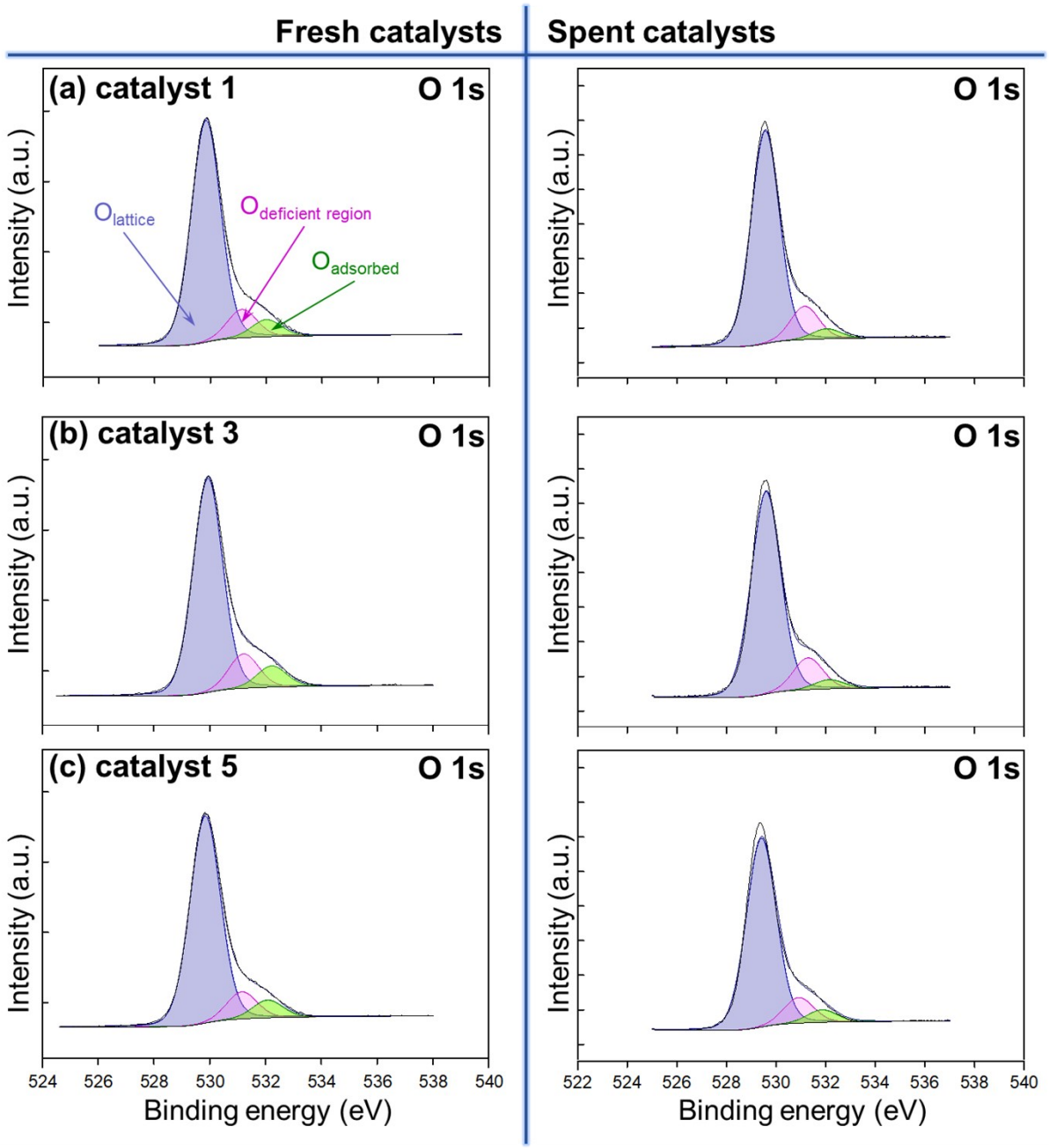

Fig. S8 XPS spectra of fresh and spent Pd-TiO_2 catalysts: $O_{lattice}$ (purple, 529.9 eV), $O_{deficient\ region}$ (pink, 531.3 eV), $O_{adsorbed}$ (green, 532.2 eV).

Table S3 Fractions of Ti^{3+} ($2p_{3/2}$), Ti^{4+} ($2p_{3/2}$), Ti^{3+} ($2p_{1/2}$), and Ti^{4+} ($2p_{1/2}$) in fresh and spent catalysts.

	Fresh catalysts				Spent catalysts			
	Ti^{3+} ($2p_{3/2}$) (%)	Ti^{4+} ($2p_{3/2}$) (%)	Ti^{3+} ($2p_{1/2}$) (%)	Ti^{4+} ($2p_{1/2}$) (%)	Ti^{3+} ($2p_{3/2}$) (%)	Ti^{4+} ($2p_{3/2}$) (%)	Ti^{3+} ($2p_{1/2}$) (%)	Ti^{4+} ($2p_{1/2}$) (%)
catalyst 1	0.64±0.1	65.40 ± 0.30	2.97 ± 0.30	31.40 ± 0.30	1.39	64.35 ± 1.81	6.24 ± 0.83	30.06 ± 0.44
catalyst 3	0.65±0.14	65.42 ± 0.20	2.82 ± 0.23	31.43 ± 0.52	1.01	64.86 ± 0.75	5.23 ± 0.56	29.66 ± 0.30
catalyst 5	0.43±0.24	65.84 ± 0.45	2.82 ± 0.30	31.13 ± 0.40	0.66	64.34 ± 1.08	4.97 ± 0.46	30.49 ± 0.42

Table S4 Fractions of $O_{lattice}$, $O_{deficient\ region}$, and $O_{adsorbed}$ in fresh and spent catalysts.

	Fresh catalysts			Spent catalysts		
	$O_{lattice}$ (%)	$O_{deficient\ region}$ (%)	$O_{adsorbed}$ (%)	$O_{lattice}$ (%)	$O_{deficient\ region}$ (%)	$O_{adsorbed}$ (%)
catalyst 1	82.56 ± 0.52	10.48 ± 0.09	6.97 ± 0.06	81.85 ± 1.43	13.48 ± 0.34	4.67 ± 1.23
catalyst 3	80.92 ± 1.50	12.10 ± 0.65	6.98 ± 0.85	83.56 ± 0.48	13.46 ± 0.35	3.79 ± 0.59
catalyst 5	82.96 ± 0.80	10.79 ± 0.02	6.26 ± 0.81	82.98 ± 0.20	12.33 ± 1.40	4.70 ± 1.19

Table S5 O_2 and CH_4 conversion, and apparent reaction rate constant (k_{app}) with TiO_2, catalyst 1, catalyst 2, catalyst 3, catalyst 4 and catalyst 5 at 723 K.

	O_2 conversion (%)	CH_4 conversion (%)	k_{app} (min^{-1})
TiO_2	30.9	50.7	7.71
catalyst 1	55.8	64.4	17.01
catalyst 2	67.0	81.9	23.10
catalyst 3	77.0	92.4	30.62
catalyst 4	75.3	93.8	29.13
catalyst 5	70.1	93.0	25.15

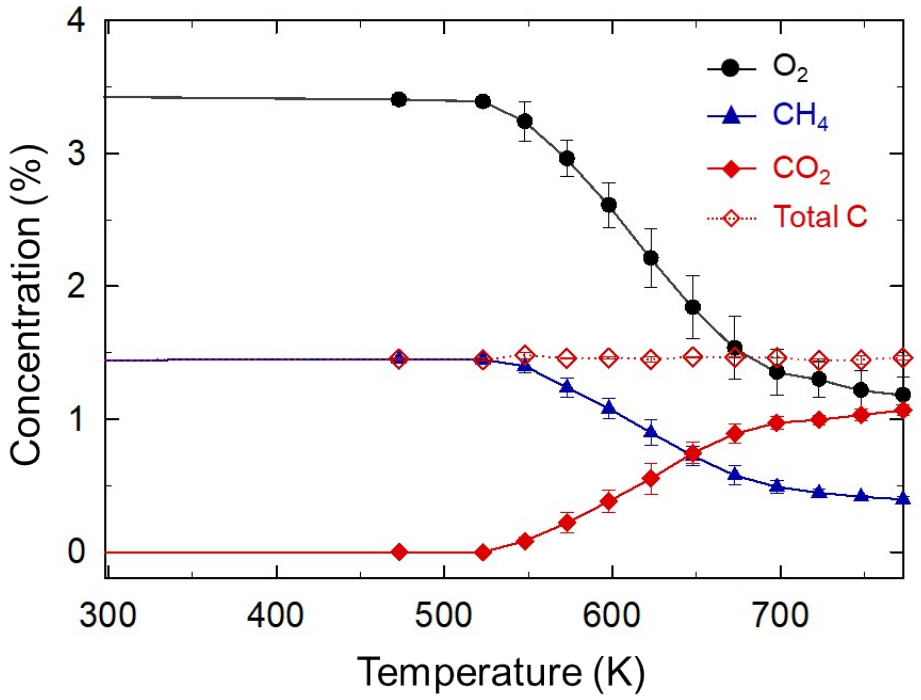

Fig. S9 The change in the concentration of O_2, CH_4, CO_2 and Total C with catalyst 3 (Helium was used instead of CO_2.).

Table S6 Reaction rates of CH_4 and $1/2O_2$ with different catalysts.

	R_{CH_4} (mmol/g_{cat}/hr)		$1/2R_{O_2}$ (mmol/g_{cat}/hr)		$\left\|\frac{R_{CH_4} - 1/2R_{O_2}}{R_{CH_4}}\right\| \times 100$ (%)[a]	
	723 K	773 K	723 K	773 K	723 K	773 K
catalyst 1	-7.16	-8.82	-7.50	-9.36	1.10	2.45
catalyst 2	-9.06	-9.87	-9.39	-10.01	0.47	2.61
catalyst 3	-10.63	-10.93	-10.35	-10.66	2.73	2.61
catalyst 4	-10.73	-11.18	-10.27	-10.71	5.00	4.84
catalyst 5	-10.41	-10.81	-9.69	-10.20	6.06	5.20

[a] Via complete CH_4 oxidation reaction ($CH_4 + 2O_2 \rightarrow CO_2 + 2H_2O$):

$$\frac{R_{CH_4}}{-1} = \frac{R_{O_2}}{-2}$$

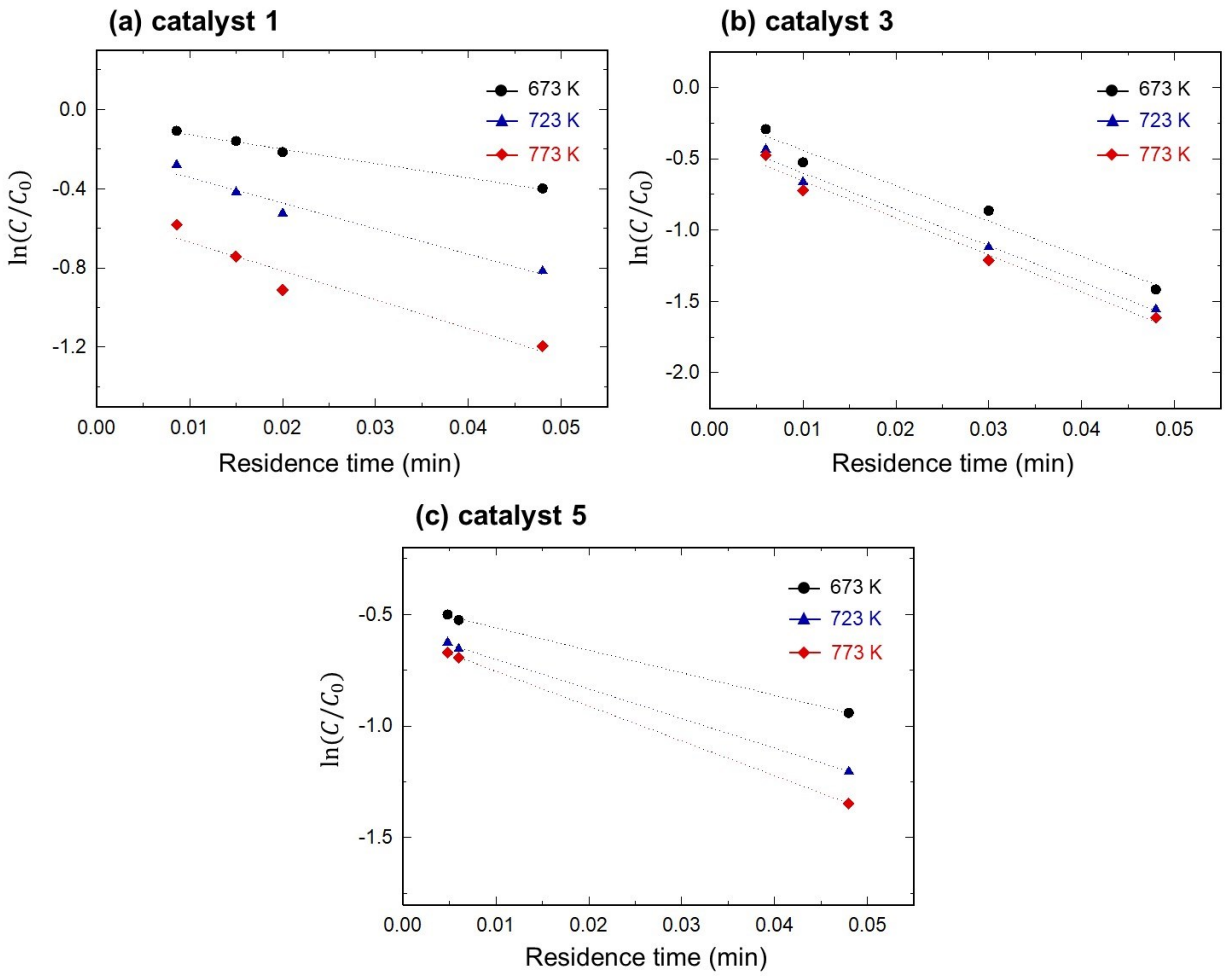

Fig. S10 The natural log of C/C_0 versus residence time (a) with catalyst 1, (b) with catalyst 3, and (c) with catalyst 5 at different temperatures.

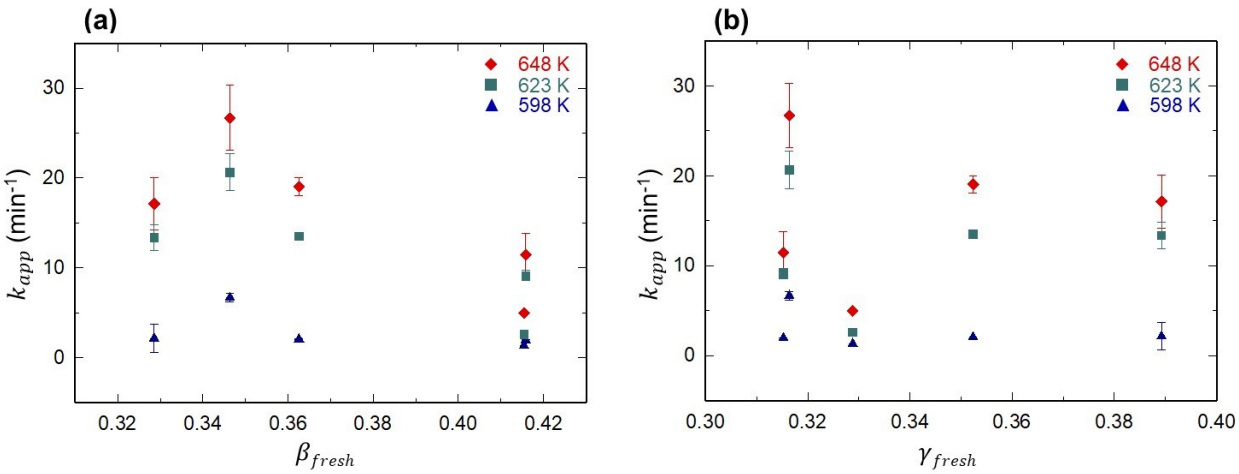

Fig. S11 Variation of the apparent reaction rate constant (k_{app}) with (a) the fraction of the total surface area of PdO (β_{fresh}) and (b) the fraction of the total surface area of PdO_x (γ_{fresh}) in the fresh catalysts at different temperatures.

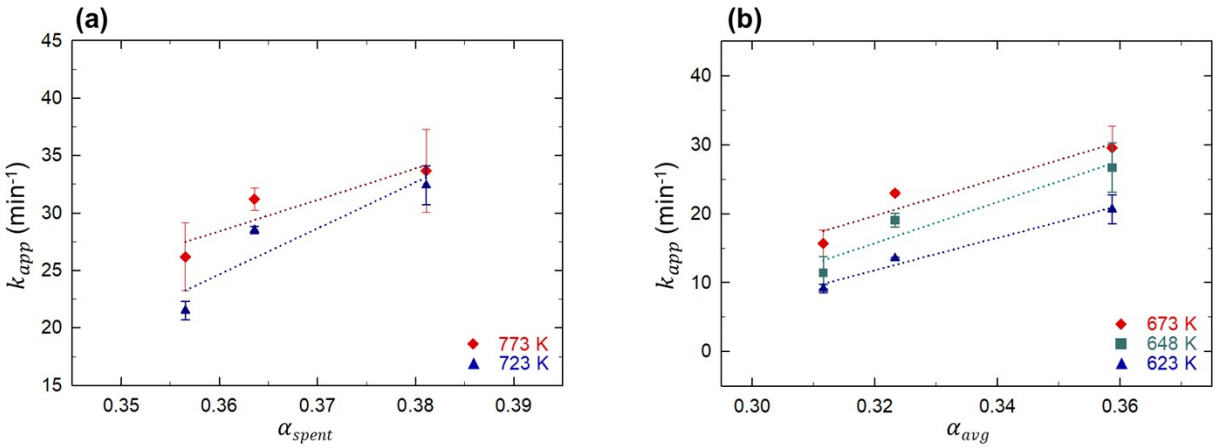

Fig. S12 Variation of the apparent reaction rate constant (k_{app}) with (a) the fraction of the total surface area of metallic Pd in the treated catalysts (α_{spent}), and (b) the average fraction of the total surface area of metallic Pd (α_{avg}) at different temperatures.

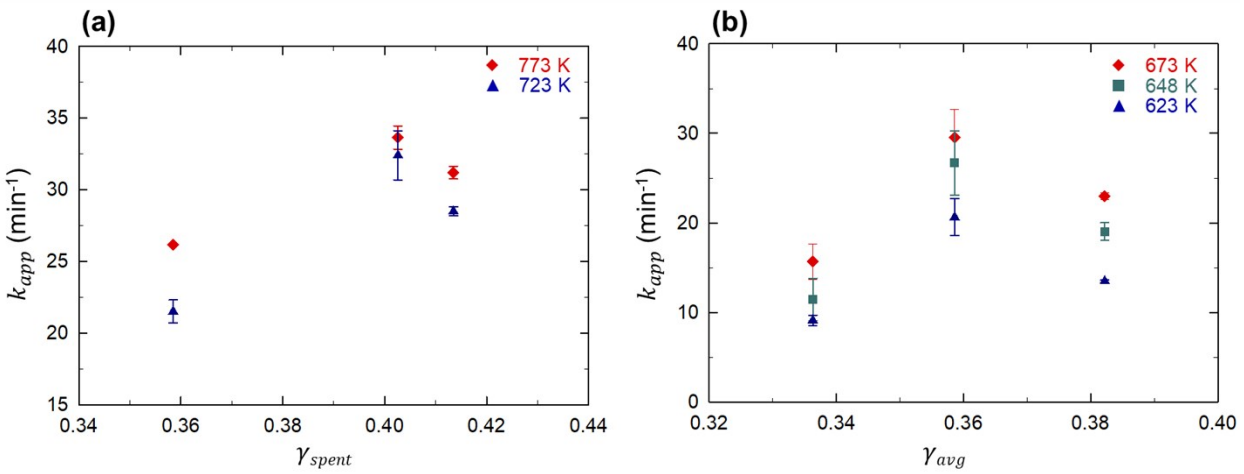

Fig. S13 Variation of the apparent reaction rate constant (k_{app}) with (a) the fraction of the total surface area of PdO_x in the treated catalysts (γ_{spent}) and (b) the average fraction of the total surface area of PdO_x (γ_{avg}) at different temperatures.

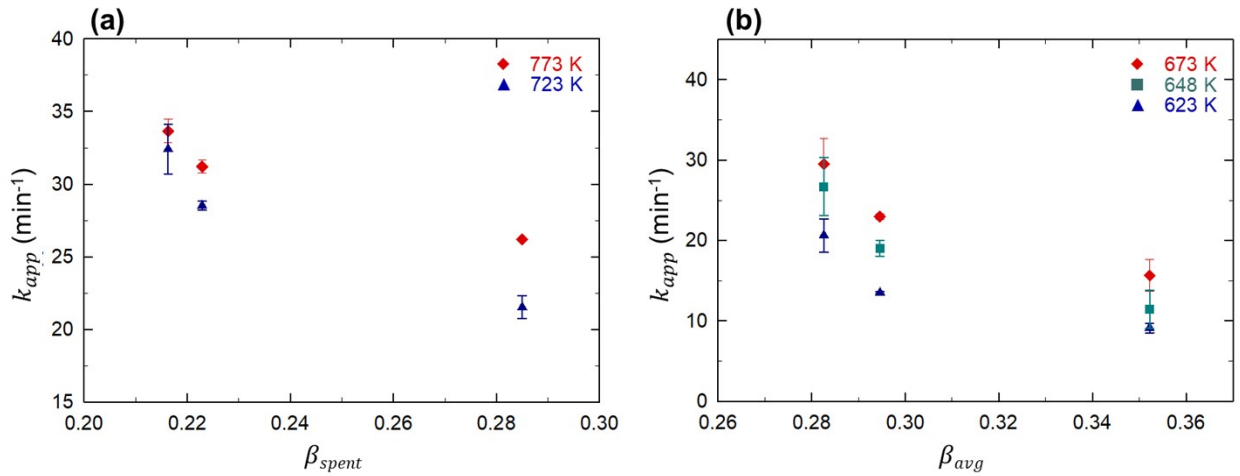

Fig. S14 Variation of the apparent reaction rate constant (k_{app}) with (a) the fraction of the total surface area of PdO in the treated catalysts (β_{spent}) and (b) the average fraction of the total surface area of PdO (β_{avg}) at different temperatures.

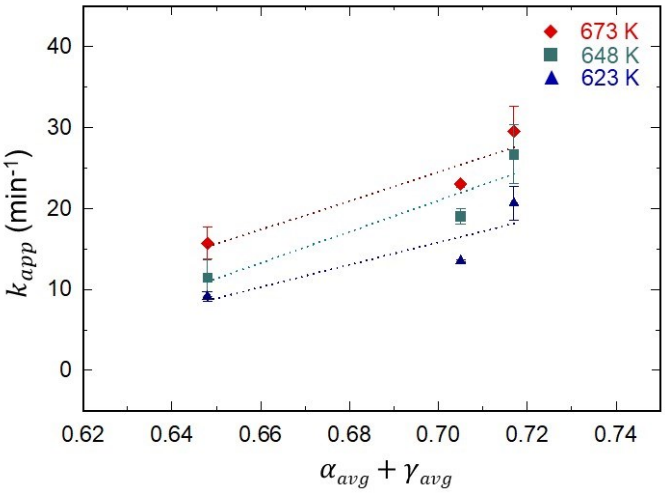

Fig. S15 Variation of the apparent reaction rate constant (k_{app}) with the sum of average fractions of the total surface area of metallic Pd and PdO_x ($\alpha_{avg} + \gamma_{avg}$) at different temperatures.

Table S7 Reaction rates of CH_4 and $1/2O_2$ with catalyst 3 under different CO_2 concentrations.

	R_{CH_4} (mmol/g_{cat}/hr)		$1/2R_{O_2}$ (mmol/g_{cat}/hr)		$\left\|\frac{R_{CH_4} - 1/2R_{O_2}}{R_{CH_4}}\right\| \times 100$ (%)	
	723 K	773 K	723 K	773 K	723 K	773 K
0% CO_2	-7.97	-8.36	-7.87	-8.35	1.32	0.09
53% CO_2	-9.21	-10.01	-9.35	-9.71	2.51	0.49
95% CO_2	-10.64	-10.95	-10.35	-10.66	2.73	2.61

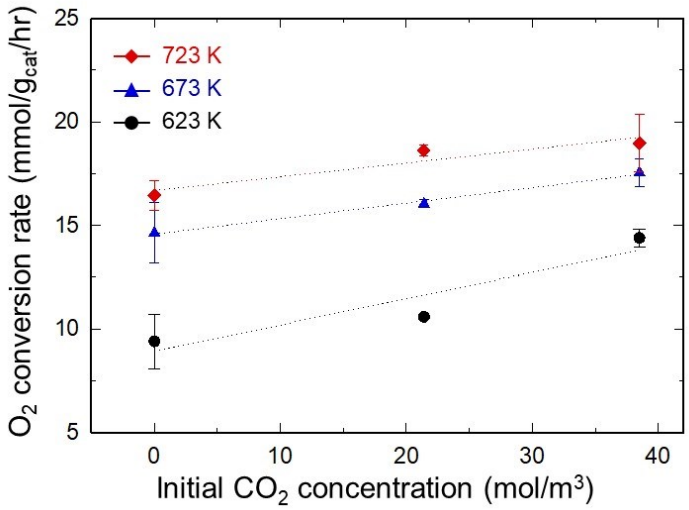

Fig. S16 Variation of O_2 conversion with CO_2 concentration at different temperatures.

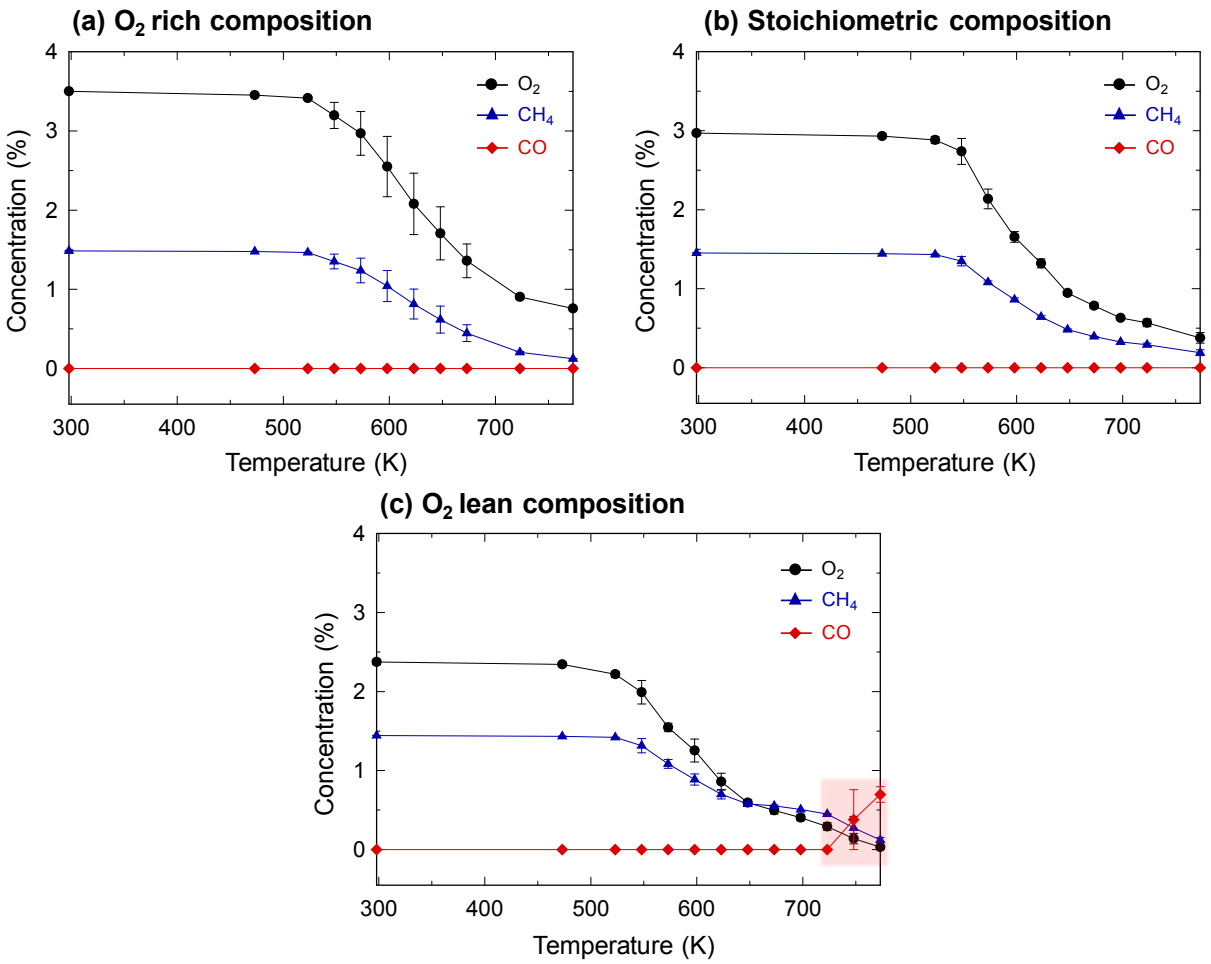

Fig. S17 (a)-(c) change in the concentration of O_2, CH_4, and CO with catalyst 3 under different initial compositions (O_2 rich composition: $O_2/CH_4 \cong 2.4$, stoichiometric composition: $O_2/CH_4 \cong 2.0$, O_2 lean composition: $O_2/CH_4 \cong 1.6$).